PCCP

PAPER

View Article Online
View Journal | View Issue

Cite this: *Phys. Chem. Chem. Phys.*, 2014, **16**, 8949

Vibronic structures and dynamics of the predissociating dimethyl sulfide and its isotopomers (CH_3SCH_3, CD_3SCD_3, CH_3SCD_3) at the conical intersection

Jun-Ho Yoon, Kyung Chul Woo and Sang Kyu Kim*

Received 11th December 2013,
Accepted 19th February 2014

DOI: 10.1039/c3cp55220a

www.rsc.org/pccp

Conical intersection seam comprised of crossing surfaces of two lowest excited states of dimethyl sulfide (DMS) has been directly accessed by the one-photon excitation from the ground equilibrium state. Since the S–C bond rupture takes place promptly, the molecular structure on the excited state effectively belongs to C_S symmetry. Namely, excited states of 1^1B_1 and 1^1A_2 in C_{2V} become $1^1A''$ and $2^1A''$ states in C_S, respectively, and the optical transition from the ground equilibrium state to the dissociating molecule at the conical intersection seam is symmetry-allowed to facilitate the nonadiabatic transition on the $2^1A''$ state, leading eventually to the CH_3S + CH_3 products. The dynamic study of DMS, in this sense, gives the great opportunity to unravel the vibronic structure of the conical intersection seam by the conventional one-photon excitation method. In this work, utilizing the photofragment excitation (PHOFEX) spectroscopic method, the vibronic structures of DMS and its isotope analogs (CD_3SCD_3, CH_3SCD_3) at the conical intersection seam have been revealed, providing accurate lifetimes and detailed dynamics associated with individual vibronic transitions. The lifetime of the excited DMS is estimated to be ~100 fs, indicating that the dissociation is complete within one single oscillation in the conical intersection region. It is also found that the symmetric CSC stretching mode is strongly coupled to the reaction coordinate, as manifested by our experimental finding that the fragmentation yield of the S–CD_3 bond is enhanced compared to that of the S–CH_3 bond in the CH_3SCD_3 dissociation reaction only when the CSC symmetric stretching vibrational mode is excited at the conical intersection region. This work demonstrates that the better understanding of the excited state could make the bond-selective chemistry into reality.

Introduction

Even though the conical intersection has been widely regarded as the dynamic funnel for nonadiabatic processes which are ubiquitous and essential in chemistry and biology,[1–6] the nature of the conical intersection in terms of its locus and dynamic role on the multi-dimensional potential energy surfaces seems to be still beyond our full understanding. Since nonadiabatic chemical reactions are governed by the dynamic passage of the reactive flux through the conical intersection, it would be fascinating if one could control the nonadiabatic reaction by manipulating the reaction path in terms of its proximity to the conical intersection. Actually, Crim and colleagues had demonstrated that the nonadiabatic transition probability in the N–H[7,8] or O–H[9] bond dissociation reaction of ammonia or phenol, respectively, could be controlled by changing the Franck–Condon active nuclear configuration on the fast dissociating excited-state through the IR + UV double resonance technique. The control of the nonadiabatic reaction by the more direct experimental probing of the conical intersection has recently been reported by our group for the S–CH_3 bond dissociation reaction of thioanisole ($C_6H_5SCH_3$).[10] In the photodissociation of thioanisole, it was found that the nonadiabatic transition probability has a peak-value at the particular vibronic transition through which the nuclear configuration in the vicinity of the conical intersection seam is effectively accessed. Nonadiabatic dynamics is extremely sensitive to the nuclear configuration of the initially prepared reactive flux as it determines the trajectory of the reaction path in terms of its proximity to the conical intersection seam.

The excited state dynamics of dimethyl sulfide (DMS) has been intensively studied especially since it was predicted that the conical intersection seam could be directly accessed by the single photon excitation.[11–16] In C_{2V}, the electronic transition from the sulfur nonbonding orbital ($3b_1$) to a Rydberg-like sulfur 4s orbital ($9a_1$) or to the C–S antibonding orbital gives

Department of Chemistry, KAIST, Daejeon 302-751, Republic of Korea.
E-mail: sangkyukim@kaist.ac.kr

rise to the $^1B_1$ and $^1A_2$ exited states, respectively.[17–20] These states are strongly mixed along the CSC asymmetric stretching coordinate, and the molecular symmetry relaxes to C_S as the prompt C–S bond cleavage occurs. Two electronic states then become A″ in C_S, and the optical excitation to both 1A″ and 2A″ states become symmetry-allowed for the dissociating molecule. These states accidentally intersect and the conical intersection seam is in the Franck–Condon region according to the theoretical calculation by the Yarkony group.[21] Namely, the conical intersection should be accessible by the single photon excitation from the ground equilibrium structure to the excited state of DMS.

It has been well established, from a number of theoretical and experimental studies, that the C–S bond cleavage of DMS is prompt and the large portion of the available energy goes into the translational energy of products.[11–16,21] Dynamic details regarding the energy disposal and vector properties of fragments have also been well investigated. Actually, as the C–S bond cleavage is the consequence of the nonadiabatic transition from the diabatically repulsive 2A″ state, the direct access to the 1A″/2A″ conical intersection seam should facilitate the S–C bond dissociation. This fact alone explains well why the S–C bond cleavage of DMS occurs instantaneously. For thorough understanding of the conical intersection dynamics, however, one should explore many different regions of the nuclear configuration space to find the dynamic correlation between the conical intersection and nonadiabatic transition probability. Surprisingly, the vibronic structure of the excited state of DMS has been only roughly known from the room-temperature gas phase absorption spectra to date.[17–20,22] Because of the ultrashort lifetime of the excited state, neither fluorescence nor multi-photon ionization spectroscopic technique could be utilized. In this work, we have employed the photofragment excitation (PHOFEX) spectroscopic technique to obtain, for the first time, the vibronic spectra of the jet-cooled DMS, DMS-d_6 (CD_3SCD_3), and DMS-d_3 (CH_3SCD_3). In the PHOFEX spectra, several distinct vibronic bands have been clearly identified, giving the homogeneously broadened line shapes for individual vibronic bands. The translational energy distributions of products are measured by the velocity-map ion imaging technique for the well-characterized vibronic transitions. In the dynamic study of DMS-d_3, the relative yields of two distinct channels are precisely determined. It is found that the S–CD_3 bond dissociation yield is enhanced compared to the S–CH_3 bond dissociation yield only when the CSC symmetric stretching mode is excited. This experimental fact demonstrates that the nuclear configuration spanned by the particular vibrational wavefunction is so critical in determining the nonadiabatic transition probability, paving a new way of the nonadiabatic reaction control.

Experiment

DMS, DMS-d_6 and DMS-d_3 were commercially purchased and used without further purification. The premixed gas containing ~94% of helium and ~6% of the sample was expanded into vacuum through a nozzle orifice (General valve 9 series, 0.5 mm diameter) with a backing pressure of 5 atmosphere. The resultant supersonic jet was skimmed through a 2 mm diameter skimmer and intersected by two counter propagating laser pulses. For the generation of collision-free condition, the vacuum chamber was differentially pumped by two turbo molecular pumps (Varian, TV 551) backed by a mechanical pump (Varian, DS 602). The photolysis laser pulse ($\Delta t \sim 5$ ns, $\Delta\bar{\nu} \approx 0.07$ cm^{-1}) in the range of 220–232.5 nm was generated by frequency doubling of a dye laser output (Sirah) pumped by a Nd:YAG laser (Spectra Physics, Quanta-ray LAB170) through a BBO crystal mounted on the homemade auto tracker. The nascent CH_3 or CD_3 radical was probed *via* the Q branch of the zero point level (0_0^0) of the $4p_z\ ^2A_2''$ Rydberg state using the (2 + 1) multi-photon excitation at 286.3 or 286.6 nm, respectively.[23] The probe laser pulse was generated by another dye laser (Lambda Physik, Scanmate 2) of which the output was frequency-doubled on a KDP crystal. The fragment ions prepared in appropriate ion optics for velocity-mapping[24] were repelled and accelerated through a 25 cm long field free region before being detected on a position-sensitive detector equipped with a 40 mm diameter MCP (Burle) coupled with a P20 phosphor screen (PHOTONIS). The two-dimensional image of a specific mass obtained by gating the front plate of MCP was recorded with a charge coupled device (CCD) camera (SONY). The central slice of 3D distribution was reconstructed by BASEX algorithm.[25] The velocity calibration was carried out with the O^+ ions from the photodissociation of O_2 at a wavelength of 224.999 nm.[26]

Computational details

Unrelaxed (rigid body) potential energy curves along two equivalent C–S bond elongation coordinates for the ground and the two lowest excited states were calculated at the complete active space second-order perturbation theory (CASPT2) level using a fully state-averaged complete active space self-consistent field (SA-CASSCF) reference wavefunction. Single point energy calculations were performed using CASPT2 for S_0, and multi-state (MS) CASPT2[27] for two A″ excited states as a function of the C–S bond length with all other nuclear degrees of freedom frozen at the optimized CASPT2 geometry of the ground state in the C_S symmetry. An active space associated with 8 electrons distributed into 7 molecular orbitals (MOs) was considered with the aug-cc-pVTZ[28,29] basis set. These orbitals contained two pairs of C–S σ/σ^* orbitals, two sulfur lone pair occupied orbitals, and the sulfur 4s Rydberg virtual orbital. The level-shift parameter of 0.3 a.u. to reach the convergence without intruder states inducing energy oscillation was optionally adapted to the CASPT2 calculation.[30] MOLPRO[31] package was used for all of SA-CASSCF and CASPT2 calculations whereas the geometry/frequency calculations and Franck–Condon simulation were carried out at the TD-B3LYP/aug-cc-pVTZ level with the Gaussian 09 *ab initio* package[32] and MolFC.[33]

Results and discussion

A. The C–S bond cleavage of DMS, DMS-d_3, or DMS-d_6 on the excited state occurs within one single oscillation period

The vibronic structures revealed in the PHOFEX spectra of DMS, DMS-d_3, and DMS-d_6 show distinct bands reflecting the

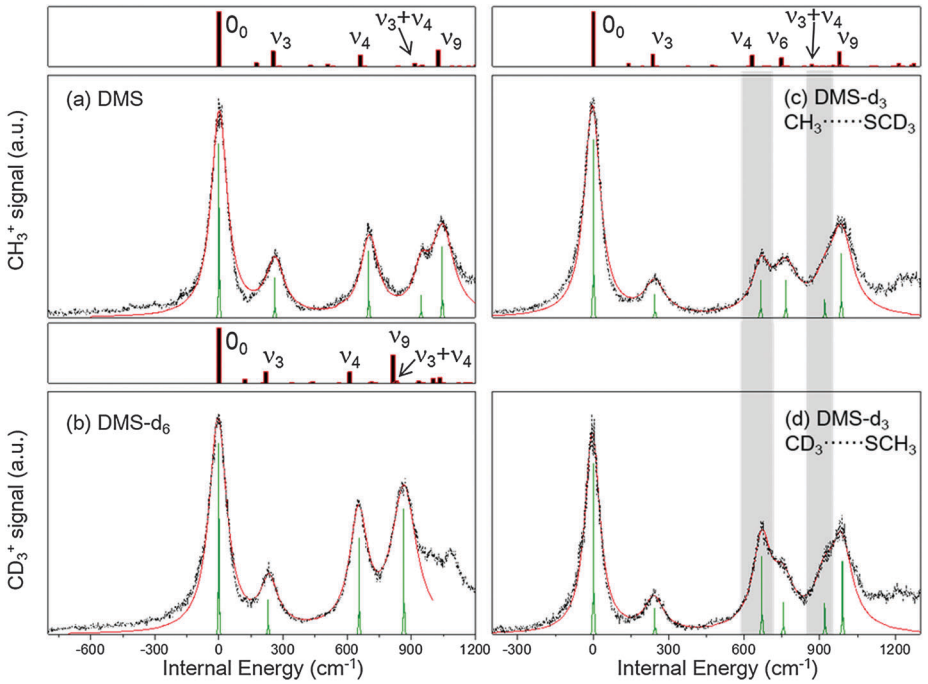

Fig. 1 PHOFEX spectra (black dashed line) of (a) DMS, (b) DMS-d_6 and (c, d) DMS-d_3 monitoring the CH_3 or CD_3 ($\nu = 0$) fragment with best-fits (red solid line) resulting from the convolutions of Lorentz functions and asymmetric rotor simulations at T_{rot} = 10 K (green stick). The spectral regions showing the relative enhancement of the CD_3 yield compared to the CH_3 yield from DMS-d_3 are denoted by gray columns. Franck–Condon simulations with spectral assignments are given in the upper traces.

structural changes and homogeneous line-broadening upon the single photon excitation, Fig. 1. From the peak position values in the PHOFEX spectra, the S_1–S_0 origin is found to be 43 879, 43 999, and 44 113 cm^{-1} for DMS, DMS-d_3, and DMS-d_6, respectively. The vibrational energies associated with individual bands match the calculated frequencies (TD-DFT with the aug-cc-pVTZ basis set) very well, giving the appropriate assignments for all observed vibronic bands. The CSC bending (ν_3), CSC symmetric stretching (ν_4), and in-plane CH_3 (CD_3) rocking (ν_9) modes are found to be active, Table 1. The observed bands show the proper H/D isotope shift consistent with the prediction of theoretical calculations. Line-shapes of individual bands except those of origins are well reproduced by the Lorentzian function, indicating that the line broadening is intrinsically homogeneous. The line shape of the origin for DMS appears to be somewhat asymmetric. Even though one is tempted to attribute this asymmetric line shape to the evidence of a certain quantum interference, the experimental fact that all the other peaks other than the origin band are well reproduced by the Lorentzian function suggests that the asymmetric shape of the origin band originates not from, for instance, the Fano-type interference. Rather, the intensity-borrowed weak absorption to the $2A''$ continuum state could be responsible for the long-tailed background PHOFEX signal observed in the energy region lower than the origin band. The contribution of the singlet-to-triplet excitation cannot be completely excluded.[35,36]

The Lorentzian fits to the individual vibronic bands give the full widths at half-maxima of $\sim$100 cm^{-1} corresponding to the lifetime of $\sim$100 fs from the uncertainty principle. The band width remains more or less constant for all vibronic bands. It is also insensitive to the CH_3/CD_3 isotopic substitution, Table 1. This experimental finding confirms that the C–S bond breaking event is prompt and occurs within one single oscillation period. This is also consistent with the theoretical prediction that the zero-point level of the excited state accesses the conical intersection region on which the nonadiabatic transition leading to the C–S bond cleavage is facilitated.[21] The vibrational excitations associated with observed vibronic bands are perpendicular to the reaction coordinate along which the zero-point level accesses the conical intersection seam, explaining well the absence of any specific mode effect on the excited state lifetime. The little isotopic substitution effect on dynamics is not surprising as the prompt C–S bond cleavage is not expected to be influenced by the secondary isotope effect.

It should be noted that the PHOFEX spectra of DMS-d_3 show quite distinct features depending on whether CH_3 or CD_3 is being probed, Fig. 1. Naturally, the peak positions and bandwidths of two PHOFEX spectra are identical for two occasions. And yet, it is found that the PHOFEX signal probing CD_3 is relatively enhanced compared to that probing CH_3 when the CSC symmetric stretching mode (ν_4) is excited. This applies also when the ν_4 + ν_3 combination mode is excited. This experimental fact suggests that one should be able to select the specific bond to be cleaved by the excitation of the appropriate vibrational mode on the edge of the conical intersection. Further discussion is in the Section C.

Table 1 Vibronic bands observed for DMS, DMS-d_6 and DMS-d_3

	DMS				DMS-d_6				DMS-d_3		
Assignment[a]	Peaks[b] (cm^{-1})	Calcd[c] (cm^{-1})	Previous studies	Γ (cm^{-1})	Peaks (cm^{-1})	Calcd (cm^{-1})	Previous study	Γ (cm^{-1})	Peaks (cm^{-1})	Calcd (cm^{-1})	Γ (cm^{-1}) CH_3/CD_3
0	0 (43 879)	0	43 965,[18] 43 840,[19] 43 879[20]	90	0 (44 113)	0	44 200[18]	100	0 (43 999)	0	77/71
ν_3	265	254		105	233	220		101	240	236	100/90
ν_4	696	662		100	655	612		100	676	631	80/85
ν_6	—	—		—	—	—		—	752	747	115/105
$\nu_3 + \nu_4$	954	915		84	—	—		—	921	868	95/95
ν_9	1040	1026		125	871	814		141	988	979	105/100

[a] ν_3: CSC bending, ν_4: CSC symmetric stretching, ν_6: in-plane CH_3 (CD_3) asymmetric rocking, ν_9: in-plane CH_3 (CD_3) symmetric rocking. (Local mode character breaks the symmetry of the normal modes for DMS-d_3. See the detail in text.) [b] Peak values. [c] TD-B3LYP/aug-cc-pVTZ values after the application of a scale factor of 0.9687.[34]

B. Energy disposal is sensitive to the initial locus of the reactive flux on the conical intersection seam

The translational energy distributions of products at several vibronic bands of DMS and DMS-d_6 are measured by the velocity-map ion imaging method, Fig. 2. As expected for the prompt dissociation reaction, the energy partitioning ratio of the total available energy to the translational energy is estimated to be 70–80% whereas the effective anisotropy factor (β) is -0.70 ± 0.10. This result is quite consistent with the earlier studies by the Aoiz group[11–16] except that our average β value is slightly lower than the previously reported value of -0.85. The interesting dynamic feature of the DMS dissociation is that the translational partitioning ratio decreases with increasing the excitation energy as clearly pointed out by a series of studies reported by the Aoiz group.[11–16] This has also been confirmed here, Fig. 2. The peak value of the total translational energy at the origin of DMS, for instance, shifts to the lower energy region at the ν_4 mode excitation at 696 cm^{-1}. This behaviour had been nicely explained by employing the "*impulsive* + *statistical*" hybrid model,[16] in which it was assumed that the bond cleavage is preceded by the intramolecular vibrational redistribution (IVR) process when the parent molecule is vibrationally excited. While this hybrid model is reasonable and widely accepted in many other cases, the ultrashort excited-state lifetime of DMS might suggest the other plausible scenario. Namely, considering the lifetime of ~100 fs and the sparse vibrational-state population of the excited DMS at the vibrational

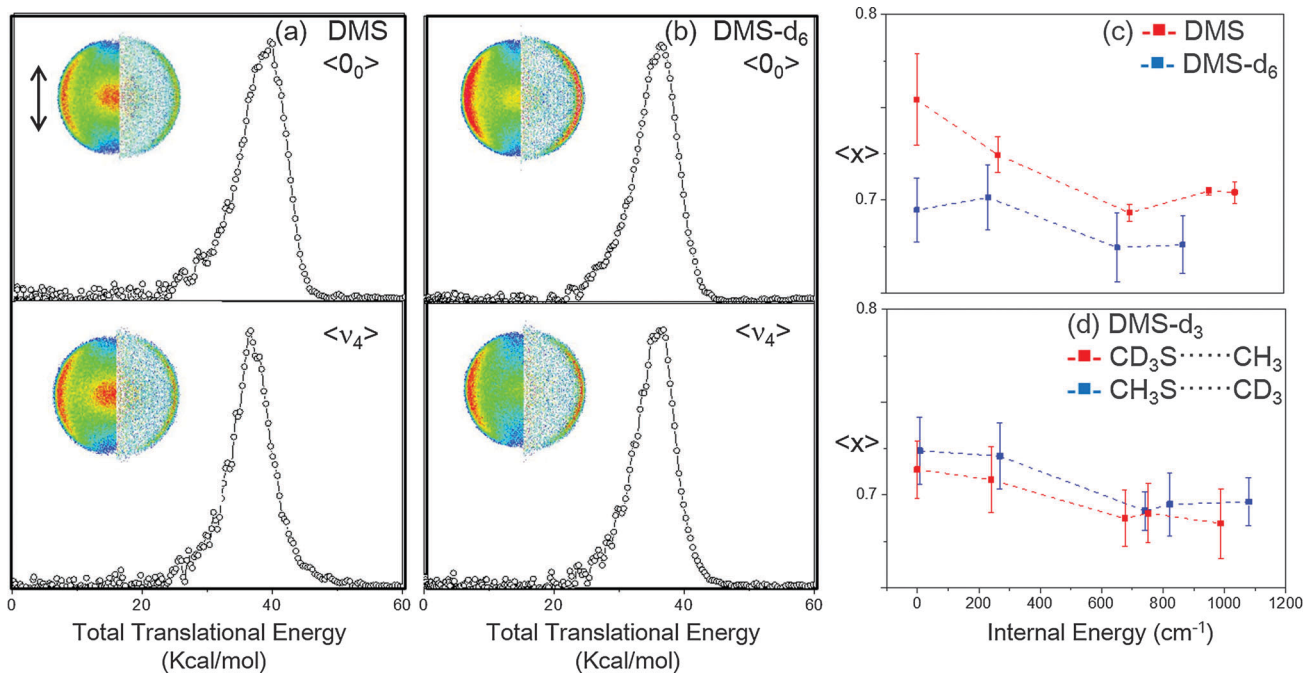

Fig. 2 Translational energy distribution and velocity map images (inset) of the (a) CH_3 and (b) CD_3 (ν = 0) fragment from the DMS and DMS-d_6, respectively, at internal energy of the origin and symmetric CSC stretching on the first absorption band. The background signal in the low energy region is attributed to the multi-photon dissociation and/or secondary dissociation of the SCH_3 (SCD_3) fragment. Raw (left) and reconstructed (right) images are also shown. The arrow indicates the polarization direction of the pump and probe laser pulses. Translational energy partitioning ratios, $\langle x \rangle$ (E_{trans}/E_{avl}, $E_{avl} = h\nu - D_0$), for (c) DMS, DMS-d_6, and (d) DMS-d_3 at the selective vibronic states are given (43 879 cm^{-1} (0_0), 44 144 cm^{-1} (ν_3), 44 575 cm^{-1} (ν_4), 44 833 cm^{-1} ($\nu_3 + \nu_4$) and 44 919 cm^{-1} (ν_9) for DMS; 44 113 cm^{-1} (0_0), 44 346 cm^{-1} (ν_3), 44 768 cm^{-1} (ν_4) and 44 984 cm^{-1} (ν_9) for DMS-d_6; 43 999 cm^{-1} (0_0), 44 239 cm^{-1} (ν_3), 44 675 cm^{-1} (ν_4), 44 751 cm^{-1} (ν_6), 44 920 cm^{-1} ($\nu_3 + \nu_4$) and 44 987 cm^{-1} (ν_9) for DMS-d_3).

energy of a few hundreds of cm^{-1}, the rate of IVR into other internal degrees of freedom is not expected to exceed the ultrafast bond dissociation rate. While it is certainly true that the vibrational energy given to the excited DMS goes into the internal energy of the SCH_3 fragment, the energy disposal mechanism may not be attributed to the fast IVR process prior to the bond cleavage event. In the photodissociation of DMS-d_3, as described above, the S–CD_3/S–CH_3 bond dissociation yield ratio increases at the ν_4 and (ν_4 + ν_3) mode excitations relative to the S–CD_3/S–CH_3 bond dissociation yield at the origin, Fig. 1. This distinct mode effect on the dissociation yield indicates that the vibrational excitation on the excited state is not randomized before the bond dissociation. If all the vibrational mode excitations end up with the identical conical intersection seam after ultrafast IVR, the specific mode effect on exit dynamics would not be observed. On the other hand, since the excited vibrational mode is perpendicular to the reaction coordinate and the bond dissociation is abrupt, it is less likely that the vibrational energy goes into the translational energy of products. Rather, the vibrational energy given to the parent excited state may dissipate into dynamically-relevant internal degrees of freedom of fragments, leading to the S–C stretching or CH_3 rocking vibrational excitation of the SCH_3 fragment, for example. The lifetime of the excited state is not long enough for the complete IVR to take place, and then the energy disposal mechanism seems to be quite complicated. At least it seems to be true for DMS that dynamic details including the energy disposal is very sensitive to the locus of the initial reactant flux on the multi-dimensional potential energy surface in the vicinity of the conical intersection. Theoretical calculation of the potential energy surfaces along the more internal degrees of freedom would help a lot for the better understanding of the ultrafast nonadiabatic bond dissociation dynamics of DMS.

C. The bond-selective chemistry is demonstrated by selecting the particular vibronic mode in the ultrafast nonadiabatic reaction of DMS-d_3

As described earlier, the S–CD_3/S–CH_3 bond dissociation yield ratio increases at the ν_4 and (ν_4 + ν_3) mode excitations relative to that at the origin for DMS-d_3. One may define the bond-selective enhancement factor for the ν_i-th mode, $\gamma(\nu_i)$, as follows.

$$\gamma(\nu_i) = \frac{I_{D,\nu_i}/I_{H,\nu_i}}{I_{D,\nu_0}/I_{H,\nu_0}}$$

Here, I_{D,ν_i} or I_{H,ν_i} represents the PHOFEX intensity at the ν_i-th mode excitation when the CD_3 or CH_3 fragment is being probed, respectively, whereas I_{D,ν_0} and I_{H,ν_0} represent the PHOFEX intensities of the respective CD_3 or CH_3 fragment taken at the origin of DMS-d_3. Whereas $\gamma(\nu_3)$, $\gamma(\nu_6)$, and $\gamma(\nu_9)$ values are all found to be ~1.0, it is found that $\gamma(\nu_4) \sim 2.0$ and $\gamma(\nu_4 + \nu_3) \sim 1.5$, as shown in Fig. 1. This experimental fact indicates that the S–CD_3 bond dissociation yield is relatively enhanced only when the CSC symmetric stretching mode (ν_4) is excited.

It should be noted that the mode-dependent enhancement observed at ν_4 and (ν_4 + ν_3) excitations is relative to the dynamic behavior at the zero-point level. Namely, the S–CD_3/S–CH_3 yield ratio at the origin of DMS-d_3 is not necessarily exactly one. The absolute yields of the CD_3 and CH_3 fragments from DMS-d_3 are not precisely measured in this work, even though they seem to be more or less same in the current experimental condition. The basic concept of the bond-selective chemistry observed here is slightly different from that behind the vibration-mediated photodissociation experiment pioneered by the Crim group.[7–9] In the latter, the overlap pattern between the ground state wavefunction with the continuum wavefunction of the upper state determines the fate of chemical reactions, making possible the selection of the chemical bond to be cleaved by tuning the ground-state vibrational mode. Here, in the case of DMS-d_3, the upper quasi-bound wavefunction is selected by the single photon excitation from the ground state. The upper state stays in the Franck–Condon region for the period shorter than ~100 fs, and the location and immediate coupling strength to the reaction coordinate are key factors determining the fate of the chemical reaction. Therefore, it is nontrivial to expect the reaction outcome from the excited-state mode selection without the full knowledge of the multi-mode coupling mechanism on the conical intersection seam. The fact that only the ν_4 mode, in the energy range here, is effective in the selective bond cleavage indicates that the corresponding CSC symmetric stretching mode is quite strongly coupled to the reaction coordinate.

Two-dimensional potential energy surface of the excited DMS with respect to the two dissociating S–C coordinates is constructed by the MS CASPT2 calculation. The calculated potential energy surface is adiabatic as a result from the coupling of 1A″ and 2A″ states, and thus it is repulsive along the both S–C bond elongation coordinates, Fig. 3. Actually, the nuclear configuration spanned by the CSC symmetric stretching mode excitation lies along the diagonal line on the two-dimensional potential energy surface. The square of the ground state (ν_4 = 1) wavefunction is depicted as red contour lines. Even though the (ν_4 = 1) wavefunction of the excited state would be somewhat different in terms of its width and depth from that of the ground state, the probability distribution of the ground (ν_4 = 1) wavefunction already indicates that the slight asymmetry in the distribution function on the edge of the repulsive potential energy surface would result in the significant difference in the branching ratio of products. It is interesting to note that the square of the (ν_4 = 1) wavefunction of DMS-d_3 is more populated toward the elongation of the S–CD_3 bond for the upper lobe located at the longer S–C bond distances, whereas it is less populated toward the S–CD_3 bond elongation for the lower lobe at the shorter S–C bond distances. This asymmetric shape of the (ν_4 = 1) wavefunction should originate from the mass unbalance between CH_3 and CD_3 moieties. This asymmetric shape should also apply to the zero-point level. The fact that the S–CD_3 bond cleavage is relatively favoured at the ν_4 mode excitation, therefore, indicates that the statistical preference for the S–CD_3 bond cleavage from the upper lobe of the (ν_4 = 1) state distribution is more effective than the statistical preference for the S–CH_3 bond cleavage originated from the lower lobe. Considering that the 1A″/2A″ avoided crossing is located at somewhat elongated C–S bond lengths according to the calculation by Manaa and

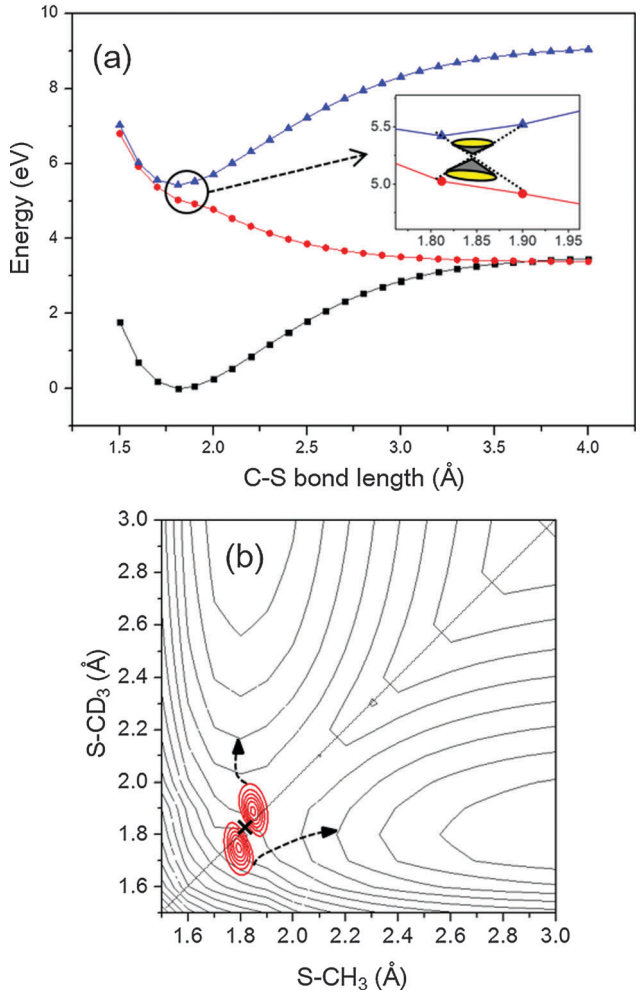

Fig. 3 (a) One-dimensional potential energy cut along the C–S bond elongation coordinates. All other geometrical parameters are frozen at the equilibrium values in the ground electronic state. The location of the conical intersection (ref. 21) is shown in the inset. (b) The square of the vibrational wavefunction (red) corresponding to the ν_4 mode of DMS-d_3 is plotted as red contours on the two-dimensional excited state potential energy surfaces (black). The wavefunction is simplified and approximated from the calculated normal mode displacement vectors with the local mode expansion based on two one-dimensional harmonic oscillator basis functions where DMS-d_3 is assumed to be a triatomic molecule and anharmonic coupling terms are neglected. Two-dimensional potential curve is plotted as a contour map with varying the S–CD_3 and S–CH_3 bond lengths in the energy range between 3.8 and 6.8 eV with a step value of 0.3 eV. The cross represents the Franck–Condon point.

Yarkony,[21] the reactive flux associated with the upper lobe of the ($\nu_4 = 1$) state distribution undergoes the C–S bond cleavage in the closer proximity of the conical intersection than the reactive flux corresponding to the lower lobe. This could be responsible for the preference of the S–CD_3 bond dissociation channel at the ν_4 mode excitation.

Conclusion

The structural and dynamic nature of the excited states of DMS and its isotope analogs (CD_3SCD_3, CH_3SCD_3) at the conical intersection seam has been revealed to give accurate lifetimes and detailed dynamics associated with individual vibronic transitions. Lifetimes of the excited DMS, DMS-d_6, and DMS-d_3 are all estimated to be ~100 fs, indicating that the C–S bond cleavage occurs within one single oscillation period in the conical intersection region. The fragmentation yield of the S–CD_3 bond is found to be ~2 times enhanced compared to that of the S–CH_3 bond in the CH_3SCD_3 dissociation reaction when the CSC symmetric stretching vibrational mode of DMS-d_3 is excited at the conical intersection region, demonstrating that the control of nonadiabatic reaction is plausible by the selective excitation of the particular mode relevant to the prompt conical intersection dynamics.

Acknowledgements

We appreciate financial support from Grants of National Research Foundation (2012-0005607, SRC 2012-0000779).

References

1 D. R. Yarkony, *Rev. Mod. Phys.*, 1996, **68**, 985–1013.
2 M. Baer, *The Role of Degenerate States in Chemistry*, John Wiley & Sons, Inc., 2003, pp. 39–142.
3 W. Domcke, D. R. Yarkony and H. Koppel, *Conical Intersections: Electronic Structures, Dynamics and Spectroscopy*, World Scientific Co. Pte. Ltd., Singapore, 2004.
4 G. A. Worth and L. S. Cederbaum, *Annu. Rev. Phys. Chem.*, 2004, **55**, 127–158.
5 D.-S. Ahn, J.-M. Lee, J.-M. Choi, K.-S. Lee, S. J. Baek, K. Lee, K.-K. Baeck and S. K. Kim, *J. Chem. Phys.*, 2008, **128**, 224305; J. S. Lim, I. S. Lim, K.-S. Lee, D.-S. Ahn, Y. S. Lee and S. K. Kim, *Angew. Chem., Int. Ed.*, 2006, **45**, 6290; I. S. Lim, J. S. Lim, Y. S. Lee and S. K. Kim, *J. Chem. Phys.*, 2007, **126**, 034306; J. S. Lim, Y. S. Lee and S. K. Kim, *Angew. Chem., Int. Ed.*, 2008, **47**, 1853.
6 D. R. Yarkony, *J. Phys. Chem. A*, 2001, **105**, 6277–6293.
7 M. L. Hause, Y. H. Yoon and F. F. Crim, *J. Chem. Phys.*, 2006, **125**, 174309.
8 M. L. Hause, Y. H. Yoon and F. F. Crim, *Mol. Phys.*, 2008, **106**, 1127–1133.
9 M. L. Hause, Y. H. Yoon, A. S. Case and F. F. Crim, *J. Chem. Phys.*, 2008, **128**, 104308.
10 J. S. Lim and S. K. Kim, *Nat. Chem.*, 2010, **2**, 627–632.
11 B. Martínez-Haya, I. Zapater, P. Quintana, M. Menéndez, E. Verdasco, J. Santamaría, L. Bañares and F. J. Aoiz, *Chem. Phys. Lett.*, 1999, **311**, 159–166.
12 P. Quintana, R. F. Delmdahl, D. H. Parker, B. Martínez-Haya, F. J. Aoiz, L. Bañares and E. Verdasco, *Chem. Phys. Lett.*, 2000, **325**, 146–152.
13 B. Martínez-Haya, F. J. Aoiz, L. Bañares, P. Quintana and E. Verdasco, *J. Phys. Chem. A*, 2000, **104**, 10150–10158.
14 B. Martinez-Haya, P. Quintana, L. Banares, P. Samartzis, D. J. Smith and T. N. Kitsopoulos, *J. Chem. Phys.*, 2001, **114**, 4450–4456.

15 J. Barr, I. Torres, L. Bañares, J. E. Verdasco and F. J. Aoiz, *Chem. Phys. Lett.*, 2003, **373**, 550–557.
16 J. Barr, I. Torres, E. Verdasco, L. Bañares, F. J. Aoiz and B. Martínez-Haya, *J. Phys. Chem. A*, 2004, **108**, 7936–7948.
17 L. B. Clark and W. T. Simpson, *J. Chem. Phys.*, 1965, **43**, 3666–3672.
18 R. McDiarmid, *J. Chem. Phys.*, 1974, **61**, 274–281.
19 W. R. Mason, *J. Phys. Chem.*, 1996, **100**, 8139–8143.
20 J. D. Scott, G. C. Causley and B. R. Russell, *J. Chem. Phys.*, 1973, **59**, 6577–6586.
21 M. R. Manaa and D. R. Yarkony, *J. Am. Chem. Soc.*, 1994, **116**, 11444–11448.
22 S. D. Thompson, D. G. Carroll, F. Watson, M. O'Donnell and S. P. McGlynn, *J. Chem. Phys.*, 1966, **45**, 1367–1379.
23 J. F. Black and I. Powis, *J. Chem. Phys.*, 1988, **89**, 3986–3992.
24 A. T. J. B. Eppink and D. H. Parker, *Rev. Sci. Instrum.*, 1997, **68**, 3477–3484.
25 V. Dribinski, A. Ossadtchi, V. A. Mandelshtam and H. Reisler, *Rev. Sci. Instrum.*, 2002, **73**, 2634–2642.
26 D. H. Parker and A. T. J. B. Eppink, *J. Chem. Phys.*, 1997, **107**, 2357–2362.
27 J. Finley, P.-Å. Malmqvist, B. O. Roos and L. Serrano-Andrés, *Chem. Phys. Lett.*, 1998, **288**, 299–306.
28 J. T. H. Dunning, *J. Chem. Phys.*, 1989, **90**, 1007–1023.
29 D. E. Woon and J. T. H. Dunning, *J. Chem. Phys.*, 1994, **100**, 2975–2988.
30 B. O. Roos and K. Andersson, *Chem. Phys. Lett.*, 1995, **245**, 215–223.
31 H.-J. Werner, P. J. Knowles, G. Knizia, F. R. Manby, M. Schütz, P. Celani, T. Korona, R. Lindh, A. Mitrushenkov, G. Rauhut, K. R. Shamasundar, T. B. Adler, R. D. Amos, A. Bernhardsson, A. Berning, D. L. Cooper, M. J. O. Deegan, A. J. Dobbyn, F. Eckert, E. Goll, C. Hampel, A. Hesselmann, G. Hetzer, T. Hrenar, G. Jansen, C. Köppl, Y. Liu, A. W. Lloyd, R. A. Mata, A. J. May, S. J. McNicholas, W. Meyer, M. E. Mura, A. Nicklaß, D. P. O'Neill, P. Palmieri, D. Peng, K. Pflüger, R. Pitzer, M. Reiher, T. Shiozaki, H. Stoll, A. J. Stone, R. Tarroni, T. Thorsteinsson and M. Wang, *Molpro, a package of ab initio programs, version 2010.1*.
32 M. J. Frisch, G. W. Trucks, H. B. Schlegel, G. E. Scuseria, M. A. Robb, J. R. Cheeseman, G. Scalmani, V. Barone, B. Mennucci, G. A. Petersson, H. Nakatsuji, M. Caricato, X. Li, H. P. Hratchian, A. F. Izmaylov, J. Bloino, G. Zheng, J. L. Sonnenberg, M. Hada, M. Ehara, K. Toyota, R. Fukuda, J. Hasegawa, M. Ishida, T. Nakajima, Y. Honda, O. Kitao, H. Nakai, T. Vreven, J. A. Montgomery, J. E. Peralta, F. Ogliaro, M. Bearpark, J. J. Heyd, E. Brothers, K. N. Kudin, V. N. Staroverov, R. Kobayashi, J. Normand, K. Raghavachari, A. Rendell, J. C. Burant, S. S. Iyengar, J. Tomasi, M. Cossi, N. Rega, J. M. Millam, M. Klene, J. E. Knox, J. B. Cross, V. Bakken, C. Adamo, J. Jaramillo, R. Gomperts, R. E. Stratmann, O. Yazyev, A. J. Austin, R. Cammi, C. Pomelli, J. W. Ochterski, R. L. Martin, K. Morokuma, V. G. Zakrzewski, G. A. Voth, P. Salvador, J. J. Dannenberg, S. Dapprich, A. D. Daniels, Ö. Farkas, J. B. Foresman, J. V. Ortiz, J. Cioslowski and D. J. Fox, *Gaussian 09, Revision A.02*, Gaussian, Inc., Wallingford CT, 2009.
33 R. Borrelli and A. Peluso, *J. Chem. Phys.*, 2003, **119**, 8437.
34 J. P. Merrick, D. Moran and L. Radom, *J. Phys. Chem. A*, 2007, **111**, 11683–11700.
35 B. F. Minaev, *J. Phys. Chem. A*, 1999, **103**, 7294–7309.
36 B. F. Minaev, I. I. Zakharov, O. I. Zakharova, A. B. Tselishtev, A. V. Filonchook and A. V. Shevchenko, *ChemPhysChem*, 2010, **11**, 4028–4034.